

Coupled Membranes with Doubly Negative Mass Density and Bulk Modulus

Min Yang,¹ Guancong Ma,¹ Zhiyu Yang,¹ and Ping Sheng^{1,2}

¹*Department of Physics, The Hong Kong University of Science and Technology, Clear Water Bay, Kowloon, Hong Kong, China*

²*Institute for Advanced Study, The Hong Kong University of Science and Technology, Clear Water Bay, Kowloon, Hong Kong, China*

(Received 9 October 2012; published 28 March 2013)

We present a structurally and conceptually simple acoustic double negative metamaterial comprising two coupled membranes. Owing to its symmetry, the system can generate both monopolar and dipolar resonances that are separately tunable, thereby making broadband double negativity possible. A homogenization scheme is implemented that enables the exact characterization of our metamaterial by the effective mass density and bulk modulus even beyond the usual long-wavelength regime, with the measured displacement fields on the sample's surfaces as inputs. Double negativity is achieved in the frequency range of 520–830 Hz. Transmission and reflection predictions using effective parameters are shown to agree remarkably well with the experiment.

DOI: [10.1103/PhysRevLett.110.134301](https://doi.org/10.1103/PhysRevLett.110.134301)

PACS numbers: 43.20.+g, 43.40.+s, 46.40.-f

The emergence of acoustic and elastic metamaterials has significantly broadened the horizon for acoustic or elastic waves. Novel phenomena such as focusing and subdiffraction imaging [1–4], near-field amplification [5], cloaking [6–9], localization of ultrasound [10], one-way transmission [11–13], and super absorption [14] have been proposed or experimentally demonstrated. At the core of these phenomena are the resonance-induced effective material characteristics such as the negative effective mass [5,15–18], negative effective modulus [19,20], or negative shear modulus [21,22].

With the realization of negative dynamic mass density in the membrane system [16] and negative modulus via the Helmholtz resonators (HR) [19], a natural extension is the doubly negative acoustic metamaterial based on the combination of the two [23]. However, coupling between the membrane and the HR is not straightforward, as the geometric symmetries of the two systems are different. Hence it is only recently that such an attempt was successfully demonstrated in the low frequency limit [24,25]. However, combining two different structures is not the only strategy to the realization of acoustic double negativity. It was shown theoretically that a single resonating unit can display overlapping responses in multiple angular momentum channels [21], including monopolar and dipolar, which are the key to the realization of acoustic double negativity [26]. Other routes to achieve double negativity, such as the geometric-induced band folding [27], have also been demonstrated theoretically and numerically.

In this Letter, we show both experimentally and theoretically the realization of double negativity in a single resonating structure, based on two coupled membranes. The work was motivated primarily by symmetry considerations. Consider a homogeneous 1D system of finite extent. The (transversely averaged) motions of two end surfaces represent two independent degrees of freedom—a symmetric mode in which the two surfaces move in phase,

and an antisymmetric mode in which the two surfaces move out of phase with each other. These two modes can characterize, respectively, the dipolar and monopolar resonances of the system. They correspond to the two effective parameters of the system because in the dipolar case there is center of mass motion and hence the corresponding resonance is denoted masslike, whereas in the monopolar case the center of mass remains stationary and only the bulk modulus plays a role; hence, it is denoted bulk moduluslike [26]. Provided the eigenfrequencies of the two resonances are tunable via system parameters, it is straightforward to realize double negativity in a desired frequency range. A distinct advantage of such a system is that, due to the simplicity and symmetry of our metamaterial, we can afford exact characterization of the system by using the measured end surface displacements, even beyond the usual long-wavelength regime [21,28,29]. From the extracted effective parameter values, the predicted transmission and reflection spectra can be compared to the experiment. In what follows we show that such a simple 1D system can indeed be realized, by coupling two membranes. While the membranes would inevitably have transverse dimensions, it is shown that in the low frequency limit where the relevant wavelength is much larger than the transverse dimension, the system is accurately 1D as far as the propagating waves are concerned.

In Fig. 1(a) we show the structure of the metamaterial that comprises two identical circular membranes, each with radius $R = 14$ mm, thickness 0.2 mm, and decorated by a circular rigid platelet (radius of 4.5 mm and mass of 159 mg) attached to the center. The two membranes are each fixed to a rigid cylindrical side wall with a radial tensile stress 1.3×10^6 Pa. They are connected by an acrylic plastic ring, which has a thickness of 1.5, inner radius 10, and height 6.0 mm. The ring has a mass of 395 mg, and the materials parameters of the membranes can be found in Ref. [14]. The amplitude and phase of the

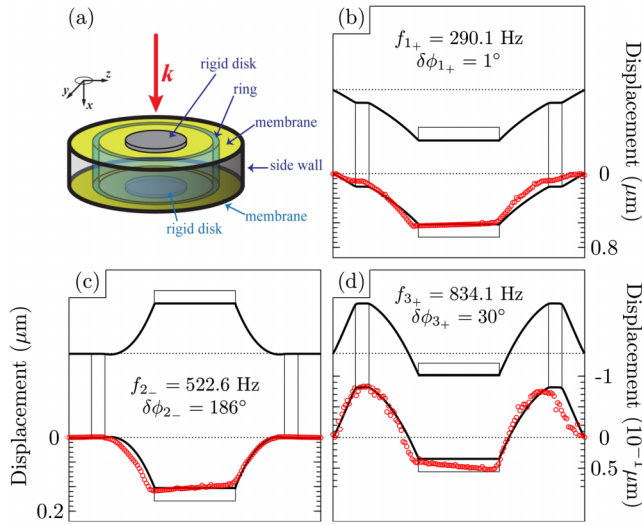


FIG. 1 (color online). (a) Schematic drawing of the metamaterial. (b) Numerically simulated (black curves) and experimentally measured (red circles) vibration profiles (eigenfunctions) of the first eigenmode. Here and in (c) and (d) circular symmetry is assumed. The rigid circular platelet is shown schematically by the hollow rectangle. (c) The second eigenmode. (d) The third eigenmode. For the third eigenmode, the relative phase is noted to be somewhat larger than that for the first mode. Here f_α is the corresponding eigenfrequency and $\delta\phi_\alpha$ the relative phase difference between the two central plates.

transmission and reflection were measured in a modified impedance tube apparatus, comprising two Brüel and Kjær type-4206 impedance tubes with the sample sandwiched in between [30]. The front tube has two sensors, plus a loudspeaker at one end to generate a plane wave in the tube. The back tube has one sensor to measure the transmitted wave. Figures 2(a) and 2(b) show the measured transmission and reflection amplitudes, respectively. Three transmission peaks, located at 290.1, 522.6, and 834.1 Hz are seen.

We limit the relevant acoustic frequency f by the condition $v_0/f = \lambda > 2R$, where $v_0 = 343$ m/sec is the speed of sound in air. Thus we have $f < 1.225 \times 10^4$ Hz under this constraint. An immediate consequence is that as far as the radiation modes are concerned, i.e., transmission and reflection, the system may be accurately considered as one dimensional. This can be seen as follows. The normal displacement u of the membrane may be decomposed as $u = \langle u \rangle + \delta u$, where $\langle u \rangle$ represents the surface-averaged normal displacement of the membrane (here $\langle \rangle$ represents surface averaging) and δu the fine details of the membrane motion. In the air layer next to the membrane surface, the acoustic wave must satisfy the dispersion relation $k_{\parallel}^2 + k_{\perp}^2 = (2\pi/\lambda)^2$, where $k_{\parallel(\perp)}$ represents the wave vector component parallel (perpendicular) to the membrane surface. Because the two-dimensional fine pattern of k_{\parallel} can be described by a linear superposition of k_{\parallel} 's, all of which must be greater than $2\pi/2R > 2\pi/\lambda$, it follows that the

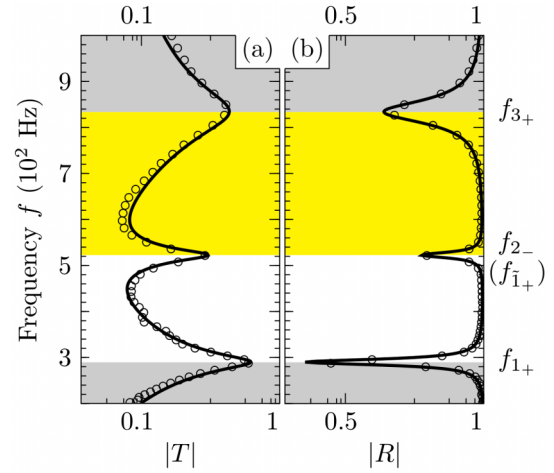


FIG. 2 (color online). (a) Transmission coefficient and (b) reflection coefficient of the metamaterial. The open circles are the experimental results obtained using the impedance measurements; the solid curves are calculated from $\bar{\rho}$ and $\bar{\kappa}$ shown in Fig. 3. Excellent agreement is seen. The band gaps are shaded gray, the double-negative passband (between 520 and 830 Hz) is light gray (yellow), and the double-positive passband is without shading.

relevant $k_{\perp}^2 < 0$. That is, the displacement component δu leads only to evanescent, nonradiating modes. The displacement component, $\langle u \rangle$, on the other hand, represents the pistonlike motion of the membrane and has k_{\parallel} components peaked at $k_{\parallel} = 0$; hence, it is coupled to the radiation modes.

Simplification to a 1D system greatly facilitates the visualization of the relevant symmetries of the two types of resonances, involving either the in-phase or the out-of-phase motion of the two membranes. An important element of our experimental measurements is the use of laser vibrometer (Graphtec AT500-05) to map the normal displacement u across the membrane on the transmission side, plus the relative phase $\delta\phi$ between the two membranes, which can be detected by the relative motion between the two platelets. In Figs. 1(b)–1(d) we show three displacement fields of the coupled-membrane system at the transmission peaks, i.e., resonance frequencies ($f_{1+} = 290.1$, $f_{2-} = 522.6$, and $f_{3+} = 834.1$ Hz). The black curves delineate the simulated results by using the COMSOL multiphysics finite element package, whereas the red circles represent the measured results using laser vibrometer. Excellent agreement is seen. For the first mode, both membranes oscillate in unison, carrying the ring together in a translational motion. For the second eigenmode, the ring is motionless and only the membranes vibrate. Because the acrylic plastic ring is rather rigid, it is impossible for the soft membrane to compress the ring at such low frequencies. Consequently, the ring acts like an anchor, and the central portions of the two membranes vibrate in an out-of-phase manner. For the third eigenmode, the ring and

the platelets vibrate in opposite phase, but the motion of the two membranes is in unison. It is seen that the simulated phase relation between the two platelets agrees with the experimental results almost perfectly.

While the first and third eigenmodes are clearly dipolar in character and hence of mass-density type (MDT), the second mode has the monopolar symmetry and hence is of bulk-modulus type (BMT) [26]. For the dipolar resonance, the total mass of the ring and the platelets serves as the most important parameter for tuning its frequency. For the monopolar resonance, the membranes' separation and transverse dimension are the crucial parameters. The fourth eigenmode is noted to be at a much higher frequency of 2976.3 Hz. Its effect in the frequency range of our interest is minimal, and therefore it is ignored in the following analysis.

The two relevant effective material parameters are the dynamic mass density $\bar{\rho}$ (arising from the symmetric mode) and the effective bulk modulus $\bar{\kappa}$ (arising from the antisymmetric mode). To extract these two effective parameters, we propose a homogenization scheme, with detailed derivation presented in the Supplemental Material [31], based on the fact that the behavior of our system is dictated by the resonant eigenmodes. The scheme needs only the three relevant eigenfunctions to delineate the correlated motions on the two ends (i.e., the two membranes). This aspect is distinct from the homogenization schemes in which matching the response of the entire frequency range of interest is required [21,32–34].

Consider the eigenfunction expansion of the scalar Green function [29],

$$G(\vec{x}, \vec{x}') = \sum_{\alpha} \frac{u_{\alpha}^*(\vec{x})u_{\alpha}(\vec{x}')}{\rho_{\alpha}(\omega_{\alpha}^2 + i\omega\beta_{\alpha} - \omega^2)}, \quad (1)$$

where angular frequency $\omega = 2\pi f$, $\rho_{\alpha} \equiv \int_{\Omega} u_{\alpha}^*(\vec{x})\rho(\vec{x}) \times u_{\alpha}(\vec{x})d\vec{x}$ denotes the averaged mass density for the α th eigenfunction $u_{\alpha}(\vec{x})$, $\rho(\vec{x})$ is the local mass density, and ω_{α} and β_{α} are the corresponding resonant frequency and dissipation coefficient. By using the experimentally measured eigenfunctions $u_{\alpha}(\vec{x})$ [as shown in Figs. 1(b)–1(d), in which circular symmetry is assumed], the relevant ρ_{α} can be evaluated from its definition. The dissipation coefficients β_{α} 's can be evaluated from the experimentally measured membrane displacement, with details shown in the Supplemental Material [31]. For the frequency range of interest, it turns out that only three eigenfunctions are needed; i.e., α ranges from 1 to 3 only. In Table I we present the relevant parameter values of the three eigenfunctions, evaluated from the measured membrane displacement as shown in Fig. 1.

By carrying out the cross-sectional average on G (denoted by $\langle G \rangle$), we obtain a symmetric component, \bar{G}_{+} , and an antisymmetric component, \bar{G}_{-} , where

TABLE I. Values of f_{α} , ρ_{α} , and β_{α} for the first three eigenfunctions.

α	1	2	3
f_{α} (Hz)	290.1	522.6	834.1
ρ_{α} (10^4 kg/m 3)	2.72	2.95	1.19
β_{α} (Hz)	10.20	12.79	49.94

$$\begin{aligned} \bar{G}_{\pm} &= \langle G(x_0, x_0) \rangle \pm \langle G(x_0, -x_0) \rangle \\ &= \sum_{\alpha=1}^3 \frac{\langle u_{\alpha}^*(x_0) \rangle [\langle u_{\alpha}(x_0) \rangle \pm \langle u_{\alpha}(-x_0) \rangle]}{\rho_{\alpha}(\omega_{\alpha}^2 + i\omega\beta_{\alpha} - \omega^2)}, \end{aligned} \quad (2)$$

and the two coordinates are now specified at the positions of the two coupled membranes. The cross-sectional averaged values of $\langle u_{\alpha}(\pm x_0) \rangle$ can be directly obtained from the laser vibrometer data (Fig. 1) for the three eigenfunctions; hence, together with the values of ρ_{α} and β_{α} (Table I) we can obtain the numerical values of \bar{G}_{\pm} for all the relevant frequencies.

Now consider a *homogeneous* 1D system of length $2x_0$. The Green function of such a 1D system is uniquely determined by the two material parameters $\bar{\rho}$ and $\bar{\kappa}$. In particular, we can have the similar quantities $\bar{G}_{\pm}^{(1D)}$ that are given by the formulas [35]

$$\bar{G}_{+}^{(1D)} = -\frac{\cot(x_0\omega\sqrt{\bar{\rho}}/\sqrt{\bar{\kappa}})}{\omega\sqrt{\bar{\rho}}\sqrt{\bar{\kappa}}}, \quad (3a)$$

$$\bar{G}_{-}^{(1D)} = \frac{\tan(x_0\omega\sqrt{\bar{\rho}}/\sqrt{\bar{\kappa}})}{\omega\sqrt{\bar{\rho}}\sqrt{\bar{\kappa}}}. \quad (3b)$$

By requiring $\bar{G}_{\pm} = \bar{G}_{\pm}^{(1D)}$, we obtain two sets of equations that determine $\bar{\rho}$ and $\bar{\kappa}$ as functions of frequency. As the solutions are multiple valued, we select the branch with the longest wavelength. Results are shown in Figs. 3(a) and 3(b). For the purpose of clarity, only the real parts of the effective parameters are plotted. The corresponding imaginary parts are shown in the Supplemental Material [31]. The frequency range in light gray (yellow) denotes the double negativity regime—520 to 830 Hz—which is noted to be fairly broad.

It should be noted that in the above homogenization scheme no use has been made of the usual long-wavelength approximation. Hence, even if the effective wavelength in our sample is comparable to $2x_0$, the relevant effective parameter values should still be accurate as far as the surface response (and hence the far-field wave field) of the system is concerned.

From $\bar{\rho}$ and $\bar{\kappa}$, we can analytically calculate the transmission and reflection coefficients T and R from the 1D model (see the Supplemental Material [31]). The results are displayed in Fig. 2 as solid curves. They are seen to agree remarkably well with the experiments (open circles) with no adjustable parameters, even beyond the

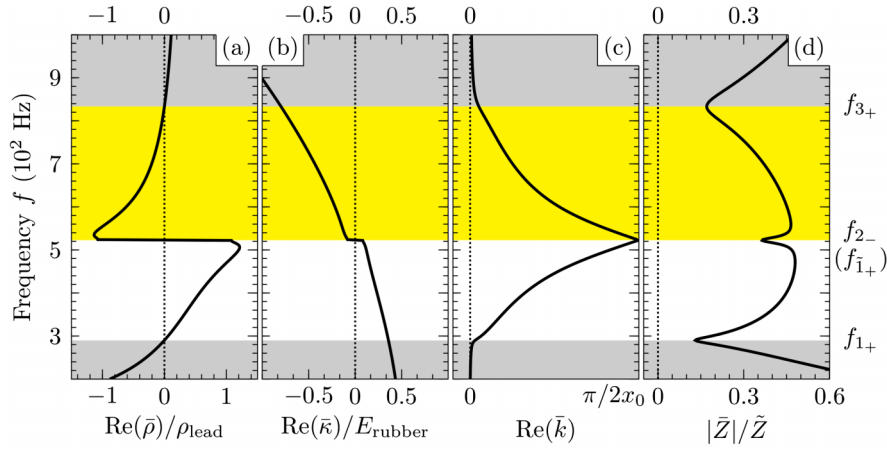


FIG. 3 (color online). Effective parameters of the metamaterial. For clarity, only the real parts of the dynamic mass density $\bar{\rho}$ (a) and effective bulk modulus $\bar{\kappa}$ (b) are shown. These effective parameters are, respectively, normalized to the static mass density of lead, $\rho_{\text{lead}} = 1.13 \times 10^4 \text{ kg/m}^3$, and the typical static Young's modulus of latex rubber, $E_{\text{rubber}} = 1.9 \times 10^6 \text{ Pa}$. The real part of the effective wave vector \bar{k} and the magnitude of the effective impedance \bar{Z} are shown in (c) and (d), respectively, with \bar{Z} normalized by $\tilde{Z} = \sqrt{\rho_{\text{lead}} E_{\text{rubber}}} = 1.5 \times 10^5 \text{ N s m}^{-3}$. The band gaps are shaded gray, the double-negative passband is light gray (yellow), and the double-positive passband is white.

usual long-wavelength regime, e.g., around f_{1+} and f_{2-} where the half wavelength is on the order of $2x_0$.

By periodically repeating the unit cells in the plane parallel to the membranes, a planar array [36–38] or a wall with overall transport properties similar to a single unit cell can be constructed. In Sec. III of the Supplemental Material [31] we give an experimental demonstration showing that the transmission and reflection characteristics of an array, comprising identically constructed units, is similar to a single cell. It confirms the fact that each cell is well isolated from its neighbors.

The transmission properties of our metamaterial are determined by two factors: impedance matching with air and the values of effective wave vectors. We notice that $\text{Re}(\bar{\rho})$ crosses zero precisely at the two eigenfrequencies f_{1+} and f_{3+} [Fig. 3(a)], arising from the two dipolar resonances. A direct consequence is that the effective impedance $|\bar{Z}| = |\sqrt{\bar{\rho}\bar{\kappa}}|$ [Fig. 3(d)] matches well with the background air. Two transmission peaks, accompanied by reflection minima (Fig. 2), are seen at f_{1+} and f_{3+} .

The antiresonance frequency, represented by f_{1+} , is located between the two MDT eigenfrequencies due to the out-of-phase hybridization of the two neighboring MDT eigenmodes that implies $\langle u(x_0) \rangle + \langle u(-x_0) \rangle = 0$ [16]. To simplify the picture, we have tuned the BMT frequency f_{2-} to coincide with the antiresonance f_{1+} to within several Hz. Owing to dissipative broadening, our calculation shows $|\bar{Z}|$ to display a small dip but the value is still fairly large in this frequency range [Fig. 3(d)] and hence mismatches with air. The transmission dip, usually expected at the antiresonance frequency f_{1+} , is effectively countered by the BMT resonance. However, the transmission peak at this frequency [Fig. 3(c)] is due to the Fabry-Perot effect of constructive interference. That is,

$\bar{k} = \pi/2x_0$ at f_{2-} , with $2x_0$ being the thickness of the metamaterial.

The key frequencies discussed above, f_{1+} , f_{1+} (f_{2-}), and f_{3+} , divide the spectrum into two passbands. The first one [white regions in Figs. 2 and 3 with $f \in (f_{1+}, f_{1+}(f_{2-}))$], is a conventional double-positive band. The second one [light gray (yellow) regions in Figs. 2 and 3 with $f \in (f_{1+}(f_{2-}), f_{3+})$], is due to the overlapping of the negative $\bar{\rho}$ and negative $\bar{\kappa}$ bands. In the doubly negative frequency regime, the effective wave vector $\bar{k} = \omega\sqrt{\bar{\rho}\bar{\kappa}}$ is real; hence, the acoustic wave is propagative. However, the wave response is out of phase to that of the double-positive medium, as can be seen from the negative slope of the dispersion in Fig. 3(c).

Single-negative band gaps are found in two regimes, $f < f_{1+}$ and $f > f_{3+}$ (the gray bands in Figs. 2 and 3). The first gap is due to negative-valued $\bar{\rho}$, whereas the second gap is due to the negative $\bar{\kappa}$. Single negativity in the effective parameters gives rise to pronounced imaginary part of the effective wave vectors within the band gaps even in the absence of dissipative effects, so that the acoustic wave must be evanescent. However, we notice that the transmission coefficients within the band gaps are not necessarily small. This is due to the relatively long decay length, given by $d = \text{Im}(\bar{k})^{-1}$. The minimum d is $\sim 13 \text{ mm}$ [31], which is still larger than the thickness of our sample. Hence the evanescent sound wave is penetrative in this case.

To conclude, we have implemented a very simple acoustic metamaterial using two coupled membranes in which the effective parameters can be exactly characterized. Double negativity in both the dynamic mass density and effective bulk modulus is achieved in a fairly broad frequency regime. The simplicity of the structure makes them suitable as the basic units for constructing acoustic

metamaterial devices with complex functionalities. Examples include but are not limited to acoustic super-lensing, acoustic Fresnel zone plates, gradient-index devices, and even near-field devices. In addition, the proposed theory framework makes extraction of effective parameters relatively simple and accurate, thereby allowing for easier and more precise control over the device properties.

This work is supported by Hong Kong RGC Grants No. HKUST 604207, No. HKUST 606611, and No. HKUST2/CRF/11G. M.Y. and G.M. contributed equally to this work.

-
- [1] J. Li, L. Fok, X. Yin, G. Bartal, and X. Zhang, *Nat. Mater.* **8**, 931 (2009).
- [2] S. Zhang, L. Yin, and N. Fang, *Phys. Rev. Lett.* **102**, 194301 (2009).
- [3] J. Zhu, J. Christensen, J. Jung, L. Martin-Moreno, X. Yin, L. Fok, X. Zhang, and F. Garcia-Vidal, *Nat. Phys.* **7**, 52 (2011).
- [4] A. Sukhovich, B. Merheb, K. Muralidharan, J. O. Vasseur, Y. Pennec, P. A. Deymier, and J. H. Page, *Phys. Rev. Lett.* **102**, 154301 (2009).
- [5] C. M. Park, J. J. Park, S. H. Lee, Y. M. Seo, C. K. Kim, and S. H. Lee, *Phys. Rev. Lett.* **107**, 194301 (2011).
- [6] S. Zhang, C. Xia, and N. Fang, *Phys. Rev. Lett.* **106**, 024301 (2011).
- [7] B. I. Popa, L. Zigoneanu, and S. A. Cummer, *Phys. Rev. Lett.* **106**, 253901 (2011).
- [8] M. Farhat, S. Guenneau, and S. Enoch, *Phys. Rev. Lett.* **103**, 024301 (2009).
- [9] N. Stenger, M. Wilhelm, and M. Wegener, *Phys. Rev. Lett.* **108**, 014301 (2012).
- [10] H. Hu, A. Strybulevych, J. Page, S. E. Skipetrov, and B. A. van Tiggelen, *Nat. Phys.* **4**, 945 (2008).
- [11] B. Liang, B. Yuan, and J. C. Cheng, *Phys. Rev. Lett.* **103**, 104301 (2009).
- [12] B. Liang, X. Guo, J. Tu, D. Zhang, and J. Cheng, *Nat. Mater.* **9**, 989 (2010).
- [13] N. Boechler, G. Theocharis, and C. Daraio, *Nat. Mater.* **10**, 665 (2011).
- [14] J. Mei, G. Ma, M. Yang, Z. Yang, W. Wen, and P. Sheng, *Nat. Commun.* **3**, 756 (2012).
- [15] Z. Liu, X. Zhang, Y. Mao, Y. Y. Zhu, Z. Yang, C. T. Chan, and P. Sheng, *Science* **289**, 1734 (2000).
- [16] Z. Yang, J. Mei, M. Yang, N. H. Chan, and P. Sheng, *Phys. Rev. Lett.* **101**, 204301 (2008).
- [17] S. H. Lee, C. M. Park, Y. M. Seo, Z. G. Wang, and C. K. Kim, *Phys. Lett. A* **373**, 4464 (2009).
- [18] S. Yao, X. Zhou, and G. Hu, *New J. Phys.* **12**, 103025 (2010).
- [19] N. Fang, D. Xi, J. Xu, M. Ambati, W. Srituravanich, C. Sun, and X. Zhang, *Nat. Mater.* **5**, 452 (2006).
- [20] S. H. Lee, C. M. Park, Y. M. Seo, Z. G. Wang, and C. K. Kim, *J. Phys. Condens. Matter* **21**, 175704 (2009).
- [21] Y. Lai, Y. Wu, P. Sheng, and Z. Q. Zhang, *Nat. Mater.* **10**, 620 (2011).
- [22] Y. Wu, Y. Lai, and Z. Q. Zhang, *Phys. Rev. Lett.* **107**, 105506 (2011).
- [23] P. Sheng, J. Mei, Z. Liu, and W. Wen, *Physica (Amsterdam)* **394B**, 256 (2007).
- [24] S. H. Lee, C. M. Park, Y. M. Seo, Z. G. Wang, and C. K. Kim, *Phys. Rev. Lett.* **104**, 054301 (2010).
- [25] S. H. Lee, C. M. Park, Y. M. Seo, and C. K. Kim, *Phys. Rev. B* **81**, 241102 (2010).
- [26] J. Li and C. T. Chan, *Phys. Rev. E* **70**, 055602 (2004).
- [27] Z. Liang and J. Li, *Phys. Rev. Lett.* **108**, 114301 (2012).
- [28] I. V. Andrianov, V. I. Bolshakov, V. V. Danishevskyy, and D. Weichert, *Proc. R. Soc. A* **464**, 1181 (2008).
- [29] J. Willis, in *Continuum Micromechanics*, edited by P. Suquet, CISM Courses and Lectures Vol. 377 (Springer Wien, New York, 1997).
- [30] K. M. Ho, Z. Yang, X. Zhang, and P. Sheng, *Appl. Acoust.* **66**, 751 (2005).
- [31] See Supplemental Material at <http://link.aps.org/supplemental/10.1103/PhysRevLett.110.134301> for details on (1) the homogenization scheme, (2) the approach to evaluating the relevant parameter values from experimental data, and (3) experimental demonstration and data for a planar array of coupled membrane oscillators.
- [32] Y. Wu, Y. Lai, and Z. Q. Zhang, *Phys. Rev. B* **76**, 205313 (2007).
- [33] X. Zhou and G. Hu, *Phys. Rev. B* **79**, 195109 (2009).
- [34] D. R. Smith and J. B. Pendry, *J. Opt. Soc. Am. B* **23**, 391 (2006).
- [35] J. Mathews and R. L. Walker, *Methods of Mathematical Physics* (Benjamin, New York, 1970).
- [36] V. A. Fedotov, M. Rose, S. L. Prosvirnin, N. Papasimakis, and N. I. Zheludev, *Phys. Rev. Lett.* **99**, 147401 (2007).
- [37] T. Driscoll, D. N. Basov, W. J. Padilla, J. J. Mock, and D. R. Smith, *Phys. Rev. B* **75**, 115114 (2007).
- [38] K. Aydin, I. M. Pryce, and H. A. Atwater, *Opt. Express* **18**, 13407 (2010).

Supplementary Information on

“Coupled Membranes with Doubly Negative Mass Density and Bulk Modulus”

by

Min Yang , Guancong Ma, Zhiyu Yang and Ping Sheng

I. Exact Effective Parameters Characterization Using Surface Response

The purpose of a homogenization scheme is to extract a small number of effective parameters for the efficient description of composite properties as perceived by an external observer. In the present case, we employ the motions at the two bounding surfaces as the central element in our approach.

From either numerical simulation (solid curves in Fig. 1) or experimental measurements, such as those by laser vibrometer (open circles in Fig. 1), the eigenstates $\{u_\alpha(\bar{x})\}$ of the composite material form an orthonormal complete set for any of its possible motion field $u(\bar{x})$. Here u denotes the normal displacement of the 1D system along the k^{th} direction. For each eigenstate, a generalized mass density is defined as

$$\rho_\alpha \equiv \int_{\Omega} u_\alpha^*(\bar{x}) \rho(\bar{x}) u_\alpha(\bar{x}) d\bar{x}, \quad (\text{S1a})$$

resonance angular frequency $\omega_\alpha = 2\pi f_\alpha$ is given by

$$\omega_\alpha^2 \equiv - \int_{\Omega} u_\alpha^*(\bar{x}) \frac{\partial}{\partial x_i} \left(C_{ikkm}(\bar{x}) \frac{\partial}{\partial x_m} \right) u_\alpha(\bar{x}) d\bar{x} / \rho_\alpha, \quad (\text{S1b})$$

where summation over indices i and m is assumed; and generalized dissipation coefficient (for $\beta_\alpha \ll \omega_\alpha$) is given by [1]

$$\beta_\alpha \equiv \int_{\Omega} u_\alpha^*(\bar{x}) \frac{\partial}{\partial x_i} \left(\eta_{ikkm}(\bar{x}) \frac{\partial}{\partial x_m} \right) u_\alpha(\bar{x}) d\bar{x} / \rho_\alpha. \quad (\text{S1c})$$

Here $\rho(\bar{x})$ is the spatial distributed mass density for the heterogeneous composite, and

$C_{ikkm}(\vec{x})$ and $\eta_{ikkm}(\vec{x})$ are the 4th-ranked tensors for its elastic modulus and dissipation coefficients, respectively, specialized to the case when all the displacements are along the k^{th} direction. These quantities provide a formal eigenfunction expansion for the Green function [2-4]:

$$G(\vec{x}, \vec{x}') = \sum_{\alpha} \frac{u_{\alpha}^*(\vec{x})u_{\alpha}(\vec{x}')}{\rho_{\alpha}(\omega_{\alpha}^2 + i\omega\beta_{\alpha} - \omega^2)}. \quad (\text{S2})$$

It is seen from Eq. (S2) that each term in the summation is dominant in the frequency regime around its eigenfrequency ω_{α} . Hence, for the purpose of investigation in our finite (and low) frequency range, only a few eigenstates are needed.

As argued in the text, as long as we are interested only in the propagating radiation modes, the problem is effectively one-dimensional (1D). For a 1D system, the external wave field is only sensitive to the motion of the two bounding surfaces. By averaging over the cross section, a set of 1D surface response functions can be obtained as

$$\bar{G}_{\pm} = \langle G(x_0, x_0) \rangle \pm \langle G(x_0, -x_0) \rangle = \sum_{\alpha} \frac{\langle u_{\alpha}^*(x_0) \rangle \langle u_{\alpha}(x_0) \rangle \pm \langle u_{\alpha}(-x_0) \rangle}{\rho_{\alpha}(\omega_{\alpha}^2 + i\omega\beta_{\alpha} - \omega^2)}, \quad (\text{S3})$$

where the symbol $\langle \rangle$ stands for surface averaging, and $\pm x_0$ denote the positions of the two bounding surfaces.

Now consider a homogeneous 1D sample with length $2x_0$. The eigenfunctions of such a system are simply given by

$$\bar{u}_{\alpha}(x) = \sqrt{\frac{1}{x_0}} \cos\left(\frac{\alpha\pi(x+x_0)}{2x_0}\right), \quad \alpha = 1, 2, 3, \dots$$

with $\bar{u}_0(x) = \sqrt{1/2x_0}$. The relevant eigenfrequencies are given by $\bar{\omega}_{\alpha} = \alpha\pi\sqrt{\bar{k}/\bar{\rho}}/(2x_0)$. Here \bar{k} and $\bar{\rho}$ are the bulk modulus and mass density of the homogeneous system. If we require the external wave response of this homogeneous 1D system to be identical to that of our experimental system, it is obvious that such a requirement can be accurately satisfied since the

external wave field is sensitive only to the motion of the two bounding surfaces, and we have exactly two effective parameters, $\bar{\kappa}$ and $\bar{\rho}$, for satisfying this constraint at each frequency (this also makes clear why our scheme works in 1D, but in higher dimensions the long-wavelength approximation becomes necessary). It turns out that for the 1D homogeneous systems, the eigenfunction expansion of the Green function can be analytically evaluated, with the results shown in the text, reproduced here for completeness:

$$\bar{G}_+^{(1D)} = -\frac{\cot(x_0\omega\sqrt{\bar{\rho}}/\sqrt{\bar{\kappa}})}{\omega\sqrt{\bar{\rho}}\sqrt{\bar{\kappa}}}, \quad (\text{S4a})$$

$$\bar{G}_-^{(1D)} = \frac{\tan(x_0\omega\sqrt{\bar{\rho}}/\sqrt{\bar{\kappa}})}{\omega\sqrt{\bar{\rho}}\sqrt{\bar{\kappa}}}. \quad (\text{S4b})$$

The homogenization condition is then simply

$$\bar{G}_\pm = \bar{G}_\pm^{(1D)}. \quad (\text{S5})$$

Substitution of Eq. (S4) into Eq. (S5) leads to analytical solutions for the effective dynamic mass density and the effective bulk modulus as

$$\bar{\rho}(\omega) = \frac{\arctan(\sqrt{\bar{G}_-}/\sqrt{-\bar{G}_+})}{\omega^2 x_0 \sqrt{-\bar{G}_+} \sqrt{\bar{G}_-}}, \quad (\text{S6a})$$

$$\bar{\kappa}(\omega) = \frac{x_0}{\arctan(\sqrt{\bar{G}_-}/\sqrt{-\bar{G}_+}) \sqrt{-\bar{G}_+} \sqrt{\bar{G}_-}}. \quad (\text{S6b})$$

Here the values of \bar{G}_\pm at each frequency can be directly determined from experimentally measured surface displacement plus the values of the ρ_α (which can be easily evaluated) and β_α (see below).

The effective wave-vector \bar{k} and effective impedance \bar{Z} can also be evaluated as

$$\bar{k}(\omega) = \omega \sqrt{\frac{\bar{\rho}(\omega)}{\bar{\kappa}(\omega)}} = \frac{1}{x_0} \arctan\left(\sqrt{\bar{G}_-}/\sqrt{-\bar{G}_+}\right), \quad (\text{S7a})$$

$$\bar{Z}(\omega) = \sqrt{\bar{\rho}(\omega)\bar{\kappa}(\omega)} = \frac{1}{\omega\sqrt{-\bar{G}_+}\sqrt{\bar{G}_-}}. \quad (\text{S7b})$$

The results of these evaluations are shown in Fig. S1.

II. Evaluation of Dissipation Coefficients β_α and Mass Density ρ_α

Even with its definition in Eq. (S1c), the dissipation coefficients β_α are not easy to be determined directly since the dissipative tensor η_{ikkm} is usually not available. However, these dissipation coefficients can still be extracted from the magnitude of surface motion during wave scattering, which can be measured by laser vibrometer.

At resonance, the system is strongly coupled to either monopolar or dipolar motions, so that its surface normal displacement average at x_0 may be written as

$$\langle \tilde{u}_\alpha(x_0) \rangle = F(x_0) \bar{G}_\pm = \frac{i}{2} \omega Z_0 u_0 (1 - S_\pm) \bar{G}_\pm, \quad (\text{S8})$$

where $F(x_0)$ denotes the force acting on the material from air at x_0 , Z_0 is the impedance of air, u_0 is the maximum displacement of the incident wave, and $S_\pm = (\omega Z_0 \bar{G}_\pm + i) / (\omega Z_0 \bar{G}_\pm - i)$ are the scattering coefficients for the system for the symmetric and anti-symmetric modes (indicated by the subscript sign) [5]. Here \tilde{u}_α denotes the displacement to be that measured experimentally, instead of the normalized eigenfunction u_α .

We note that at resonance, \bar{G}_\pm is related to its eigenfunction $u_\alpha(x_0)$ as

$$\bar{G}_\pm \cong \frac{2 |\langle u_\alpha(x_0) \rangle|^2}{i \omega \rho_\alpha \beta_\alpha}. \quad (\text{S9})$$

Substitution of (S9) into (S8) leads to

$$\langle \tilde{u}_\alpha(x_0) \rangle \cong \frac{2 Z_0 |\langle u_\alpha(x_0) \rangle|^2 / \rho_\alpha}{2 Z_0 |\langle u_\alpha(x_0) \rangle|^2 / \rho_\alpha + \beta_\alpha} u_0. \quad (\text{S10})$$

Therefore, the dissipation coefficient β_α may be directly solved from Eq. (S10) as

$$\beta_\alpha = \frac{2 Z_0 |\langle u_\alpha(x_0) \rangle|^2}{\rho_\alpha} \left(\frac{u_0}{\langle \tilde{u}_\alpha(x_0) \rangle} - 1 \right). \quad (\text{S11})$$

More explicitly, if we relate \tilde{u}_α and u_α by the relation

$$u_\alpha(x_0, r) = \tilde{u}_\alpha(x_0, r) / A, \quad (\text{S12})$$

then A is given by

$$\begin{aligned} A^2 &\equiv \int_{\Omega} [\tilde{u}_\alpha(\bar{x})]^2 d\bar{x} \\ &= 4\pi \left[h_{\text{rubber}} \int_0^R |\tilde{u}_\alpha(r)|^2 r dr + h_{\text{plate}} \int_0^{r_p} |\tilde{u}_\alpha(x_0, r)|^2 r dr \right] + \\ &\quad + 2\pi h_{\text{ring}} \int_{r_1}^{r_2} |\tilde{u}_\alpha(x_0, r)|^2 r dr. \end{aligned} \quad (\text{S13})$$

The three separate integrals arise from the three separate regions that can be clearly visualized in Fig. 1. From Eq. (S11), we then obtain

$$\beta_\alpha = \frac{8\pi Z_0}{\rho_\alpha R^2} \left[\int_0^R u_\alpha(x_0, r) r dr \right]^2 \left(\frac{u_0 R^2}{2 \int_0^R \tilde{u}_\alpha(x_0, r) r dr} - 1 \right). \quad (\text{S14})$$

For the mass density ρ_α , we can evaluate its value directly as

$$\begin{aligned} \rho_\alpha &= 2 \times 2\pi h_{\text{rubber}} \int_0^R |u_\alpha(x_0, r)|^2 \rho_{\text{rubber}} r dr + \\ &\quad + 2 \times 2\pi h_{\text{plate}} \int_0^{r_p} |u_\alpha(x_0, r)|^2 \rho_{\text{plate}} r dr + \\ &\quad + 2\pi h_{\text{ring}} \int_{r_1}^{r_2} |u_\alpha(x_0, r)|^2 \rho_{\text{ring}} r dr. \end{aligned} \quad (\text{S15})$$

The evaluated ρ_α and β_α for the three relevant eigenfunctions are presented in Table I.

In the following, we show in Fig. S1 the evaluated dynamic mass density, effective bulk modulus, the effective wave vector, and the impedance of our sample, all as functions of frequency based on both numerically simulated eigenfunctions (open triangles) and experimentally measured eigenfunctions (solid curves). The imaginary parts are shown in red, the real parts in black. In Fig. S2 we show the transmission and reflection predictions obtained from the effective parameters in the homogeneous 1D model. Excellent agreement is seen.

III. Transmission Through a Planar Array

As mentioned in the text, the locally resonant nature of the coupled-membrane system enables it to be repeated and fit onto an existing wall / skeleton, forming a planar array without changing its characteristics, as long as each cell is well isolated from its neighbors. A wall comprising a large array of such unit cells can exhibit dramatic frequency dependent behavior, predictable from the effective parameters of the unit cell.

To demonstrate this, we manufactured a set of coupled-membranes systems with radius of 12 mm, the two stiff plates have radius of 4.5 mm and weight of 190 mg. In the middle we place a 10 mm height rigid ring that has a mass of 380 mg. The ring has an outer radius of 10.5 mm and thickness of 1.5 mm. Note that due to the constraints imposed by our experimental setup and fabrication ability, the unit cell's parameters are slightly different from those in the main text. By arranging five such unit cells them into a 50 mm radius circular aluminum plate (Fig. S3(a)), the intensity transmission coefficient has been measured under normal incidence (open circles in Fig. S3(b)). The measured result for a single cell is also plotted in Fig. S3(b) as red symbols. Based on the homogenized effective parameters, the amplitude transmission coefficient for the metamaterial-modified plate can be easily calculated. The results for the two cases are shown as solid curves in Fig. S3(b). Excellent agreement is seen. The similarity between the array and single cell is also each to see.

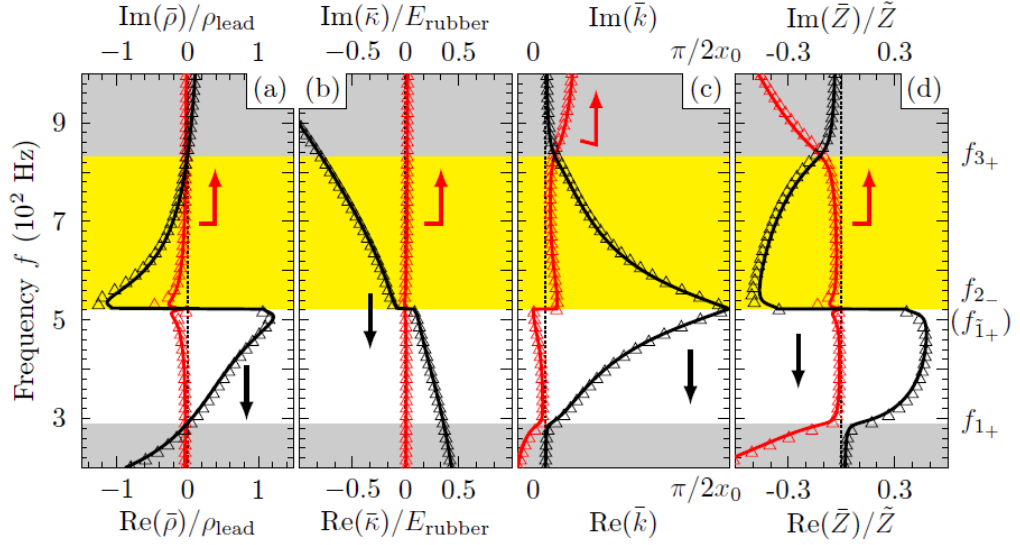


FIGURE S1. Effective parameters of the metamaterial. The dynamic mass density $\bar{\rho}$ **(a)** and effective bulk modulus $\bar{\kappa}$ **(b)** are respectively normalized to the static mass density of lead, $\rho_{\text{lead}} = 1.13 \times 10^4 \text{ kg/m}^3$, and the typical static Young's modulus of latex rubber, $E_{\text{rubber}} = 1.9 \times 10^6 \text{ Pa}$. The wave-vector \bar{k} and the effective impedance \bar{Z} are shown in **(c)** and **(d)**, respectively, with \bar{Z} normalized by $\tilde{Z} = \sqrt{\rho_{\text{lead}} E_{\text{rubber}}} = 1.5 \times 10^5 \text{ N} \cdot \text{s} \cdot \text{m}^{-3}$. The solid curves are results based on measured eigenfunctions and the open triangles are from numerically simulated eigenfunctions. Real parts of the parameters are colored in black, and imaginary parts are in red. The bandgaps are shaded in grey, the double-negative passband is colored in yellow, and the double-positive passband is in white.

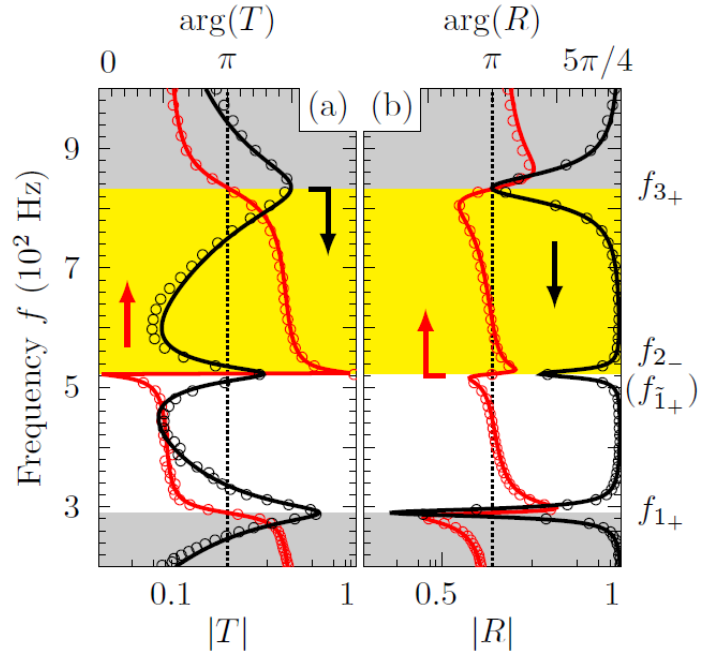


FIGURE S2. (a) Transmission coefficient and (b) reflection coefficients of the metamaterial. The open circles are the experimental results obtained using the impedance measurements, the solid curves are calculated from $\bar{\rho}$ and $\bar{\kappa}$ shown in Fig. S1. Excellent agreement is seen. Color black is standing for amplitudes and color red is for phases. The bandgaps are shaded in gray, the double-negative passband is shaded in yellow, and the double-positive passband is without shading.

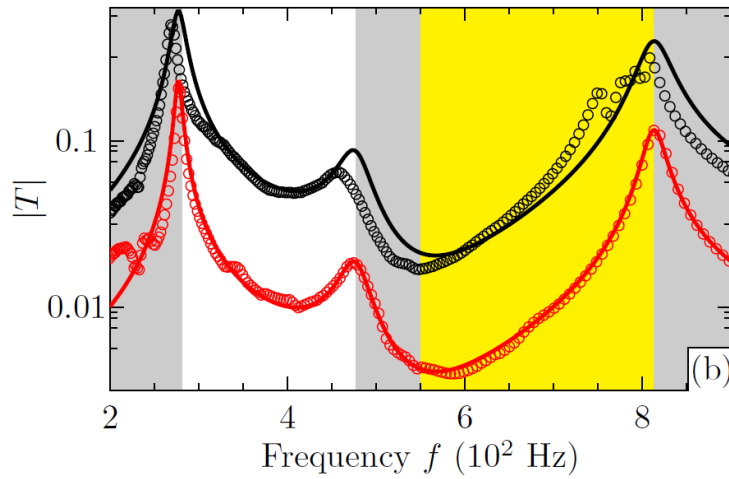
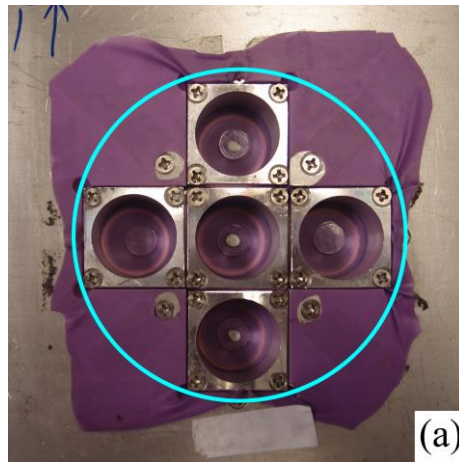


FIGURE S3. (a) A photo image of an array comprising five unit cells. The cyan circle represents the cross section of our impedance tube. (b) Normalized transmission plotted as a function of frequency f . The open circles are the experimental results obtained using the impedance measurements, the solid curves are calculated from the homogenized effective parameters. Black stands for results of five-unit planar array and red represents the transmission for a single unit cell. The bandgaps are shaded in gray, the double-negative passband is shaded in yellow, and the double-positive passband is without shading. Except for the magnitude, the similarity of the two curves is clearly seen, thereby confirming the good isolation between the unit cells.

References

- [1] L. Landau and E. Lifshitz, Theory of elasticity," (Pergamon Press, 1989) Chap. 5, p. 135.
- [2] J. Mathews and R. Walker, Methods of mathematical physics," (Addison-Wesley, 1970)
Chap. 9, p. 267.
- [3] Courant and Hilbert, Methods of mathematical physics 2 vols," (John Wiley & Sons, 1989)
Chap. 5, p. 360.
- [4] J. Willis, in *Continuum Micromechanics*, edited by P. Suquet, CISM Courses and Lectures
No. 377 (Springer Wien, New York, 1997).
- [5] D. Keefe, R. Ling, and J. Bulen, The Journal of the Acoustical Society of America 91, 470
(1992).